

Low Order Complexity Vision-Based Docking

Brian W. Minten, Robin R. Murphy, Jeff Hyams, Mark Micire

Abstract—This article reports on a reactive docking behavior which uses a vision algorithm that grows linearly with the number of image pixels. The docking robot imprints (initializes) on a two-colored docking fiducial upon departing from the dock, then uses region statistics to adapt the color segmentation in changing lighting conditions. The docking behavior was implemented on a marsupial team of robots, where a daughter micro-rover had to re-enter the mother robot from an approach zone with a 2 meter radius and 140° angular width with a tolerance of ±5° and ±2cm. Testing during outdoor conditions (noon, dusk) and challenging indoor scenarios (flashing lights) showed that using adaptation and imprinting was more robust than using imprinting alone.

Keywords— docking, artificial intelligence, control, multi-agents, vision-based robotics

I. INTRODUCTION

Much of the initial focus with multi-agent teams has been on strategies for the deployment and cascaded control of members over large distances, ignoring the specific issue of how to collect the agents back into one unit. Docking the agents, however, is essential for recovery, recharging, and sample processing. It also allows robots to physically cooperate or reconfigure so that they may connect and achieve a mobility or mission advantage. The use of human teleoperation for final docking maneuvers is an undesirable solution because it requires an open (and therefore, potentially detectable and corruptible) communication channel, and it may lead to cognitive strain for the operator.

Docking is especially important for a class of cascaded heterogeneous robots called *marsupials*, where a “mother” agent transports one or more “daughter” micro-rover agents to a mission site. [4], [8] Without docking, the mother agent cannot recover the daughter, service it, or transport it home or to a new task site.

Docking is a challenging problem for several reasons, most notably the need to accurately extract both relative position and orientation. [1] This article reports on a vision-based docking behavior that:

1. Offers low order complexity (is linear in the number of image pixels for the average case),
2. Uses a color segmentation algorithm that is lighting insensitive due to its use of the Spherical Coordinate Transform [10] and adaptive segmentation [3],
3. Requires no explicit communication between docker and dockee,
4. Is reactive, and therefore compatible with reactive and hybrid deliberative/reactive architectures, plus embedded systems, and

5. Has been shown to be faster than teleoperation with a similar success rate.

II. RELATED WORK

The pattern of actions comprising how a single agent can dock was originally explored by Arkin and Murphy [1] in 1990, producing a reactive, potential fields style of behavior for docking. Much of the subsequent docking research [5], [6], [7], [9], [11] either duplicates these results or produces more computationally complex methods. Spofford et al. [8] also deals with docking, but is primarily concerned with agents’ vision abilities, rather than integration with motion control. Our current work is an extension of our earlier contributions to [1]. The original approach used combinations of potential fields encapsulated in a motor schema to dynamically control docking without explicit path planning. The robot’s motion is computed instantaneously as a function of moving to the correct orientation (tangential to the dock) and relative depth (attraction). This motor schema had low computational complexity, making it suitable for a daughter, as long as a low-order complexity vision algorithm could be found. In the 1990 work, the pose of the robot relative to the dock was extracted from a black and white image of a large square landmark using the inverse perspective transform.

The work presented in this article differs from that described above primarily in the visual component. The vision system in this article is color-based, and it uses the change in the number of pixels between two colored regions to guide the robot.

III. APPROACH

The general approach to the docking behavior follows [1], which divided the area around a dock into four sub-areas as shown in Fig. 1. It is assumed that the daughter will move to the mother using a GPS location or other *a priori* location. The sub-area over which the daughter is moving towards the mother but cannot perceive her is called the *Ballistic Region*, because the daughter is operating under a ballistic control regime. Once the daughter perceives the mother, she has entered a closed-loop control regime which forms the *Controlled Region*. The Controlled Region is divided into two zones: *Coercive* and *Approach*. In the Coercive Zone, the daughter is directed, or coerced, to the docking portion of the mother by a tangential force. Once the daughter sees the dock, she is in the Approach Zone and can begin to move towards the dock and align herself properly. The width of the Approach Zone is a function of the perceptibility of the dock; in [1], the optics dictated a 60° Approach Zone, while in this article, the optics supported 140°. Finally, this system dictated a final Dead Reckoning Zone, where the daughter had to back

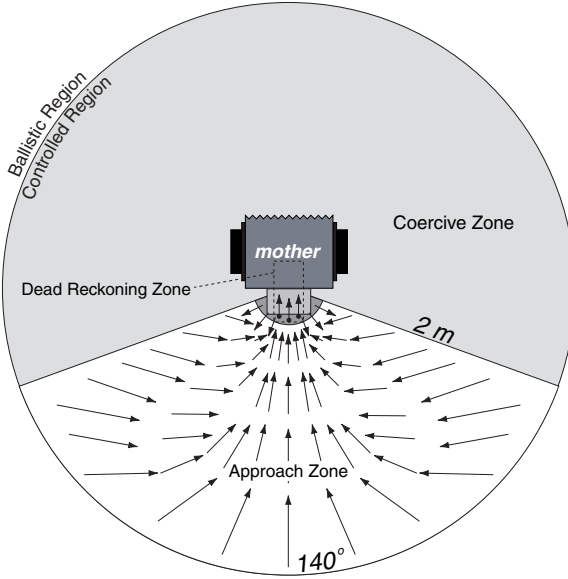


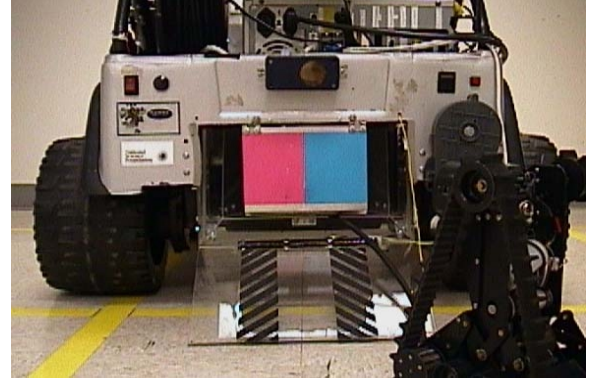
Fig. 1. Docking regions and potential field within the approach zone.

into the mother without the benefit of the camera. (Notice in Fig. 2 that the dock is at the rear of the mother, with the daughter tilting her camera so as to look backwards while in the Approach Zone.) The entire sequence, from Ballistic through the Approach Zone, is referred to in [1] as the docking behavior. Our effort is concerned only with the behavior of the daughter in the Approach Zone. To distinguish our docking behavior from the larger behavior, we refer to ours as the “close dock” behavior.

Our implementation follows [1], where a behavior is divided into two schema: a *perceptual schema*, which detects the stimulus, and a *motor schema*, which produces the observable actions that the daughter takes to dock. The docking behavior is reflexive (stimulus-response). As shown in Fig. 3, the perceptual schema supplies perspective and size cues extracted from an artificial landmark to the motor schema, which computes a vector and translates this into drive commands for skid steering.

IV. PERCEPTUAL SCHEMA

The perception for the close dock behavior relies on three concepts. First, the pose estimation is based on perspective and looming extracted from a landmark or fiducial. Second, in order to be insensitive to changes in outdoor lighting conditions, the perceptual schema uses the Spherical Coordinate Transform. [10] This color space was shown by Hyams, Powell, and Murphy [2] to be insensitive to differing light sources, shadows, and highlights compared with HSI and RGB spaces. Third, the perceptual schema also compensates for apparent changes in color by *imprinting*, or acquiring the true colors of the docking landmark in the deployed environment, as the daughter exits the mother, and then *adapting* the region thresholds to changes in lighting using an extension of work by Murphy.[3]



a.



b.

Fig. 2. The marsupial mother a) displaying the fiducial to allow the daughter to dock; and b) with the daughter inside.

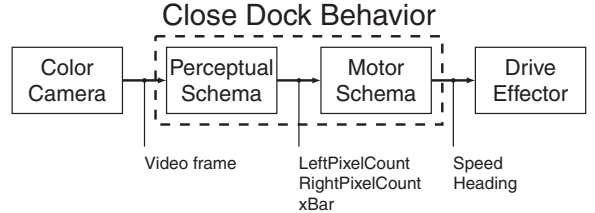


Fig. 3. An overview of the docking behavior.

A. Spherical Coordinate Transform

The docking behavior relies heavily on the accuracy with which the fiducial can be segmented. Unfortunately, color segmentation is notoriously dependent on lighting conditions, especially illumination. The color segmentation algorithm combats this problem by using the Spherical Coordinate Transform (SCT). Segmentation using SCT has been shown to perform well when subjected to fluctuations of image intensity caused by varying lighting conditions. This was originally explored in the medical imaging community,[10] and has more recently also proven useful in the field of robotics. [2]

The SCT segmenter is a general-purpose color image segmenter that is computationally inexpensive and simple to

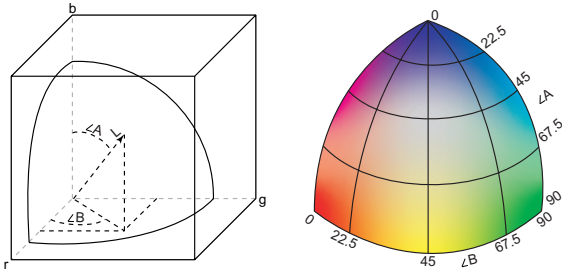


Fig. 4. A color represented by the vector L (left); the spherical shell (right).

implement. The spherical coordinate transform is defined as:

$$L = \sqrt{r^2 + g^2 + b^2}$$

$$\angle A = \cos^{-1} \left[\frac{b}{L} \right]$$

$$\angle B = \tan^{-1} \left[\frac{g}{r} \right]$$

where L is intensity, and A and B represent color independently from intensity. If a particular color is plotted as a point in rgb space (see Fig. 4), then the magnitude of the vector to the point is L , the angle between the vector and the blue axis is A , and the angle between the red axis and the projection of the vector onto the rg plane is B . The resulting color space defined by the transformation is an octant of a spherical shell. In this context, color can be defined as the point within the octant that the vector passes through.

SCT has useful properties other than lighting independence. Color space representations such as HSI, while offering intensity invariance, make it difficult to segment colors as they tend toward gray. A slight variation in color balance may cause the hue to change radically. In contrast, SCT allows trivial segmentation for these colors, as well. Gray appears in the middle of the color triangle of Fig. 4, easily bounded by ranges of A and B .

B. Feature Extraction Algorithm

After the SCT has been performed, the image is segmented separately for the colors of the left and right fiducial blocks. In spherical space, this task reduces to checking to see whether A and B fall within the ranges defining either color. Next, a hash-table-based connected components algorithm is applied to the two resultant binary images. With components now appropriately labeled, analysis proceeds with computing of component centers and sizes. This entire algorithm has average case order complexity that is linear with the number of image pixels or $O(n \times m)$, where n, m are the number of rows and columns, respectively, in the image.

The motivation for using connected components was to prevent items that have color similar to that of the fiducial, and happen to be in the image, from contributing to the pixel counts. To be considered, each component must

be larger than a set number of pixels, 20 being an empirically determined reasonable value based on the landmark size and optics. The difference between the horizontal positions of the leftmost pixel in the right block, and the rightmost pixel in the left block must also be within a limits, set loose enough to allow some amount of roll on the daughter's approach. Finally, both components must be adequately vertically aligned within the image. When all these conditions are met, the component pair is a possible match to the fiducial. If there is more than one match, the pair with the ratio of pixel counts closest to 1.0 is chosen. As a result, only relatively balanced blocks of color with the correct orientation are considered.

C. Imprinting and Adaptation

While SCT provides for segmentation with a good degree of lighting *intensity* independence, changes to the *balance* of impinging light sources (e.g., those that may be caused by direct vs. indirect sunlight when under shadow or cloud cover) have the effect of changing the perceived color of the fiducial. To cope with this problem, the daughter imprints on the fiducial colors as she departs for the mission. Good alignment is assumed, and two pixel blocks which should lie in the middle of each block are sampled for initial color statistics (mean and standard deviation of A and B).

One of the caveats of the imprinted statistics is that they are taken over a short time span. Thus, in highly uniform lighting, very small allowable color ranges may result. If a portion of the fiducial becomes shadowed on approach, it is highly possible that only a portion of the color block will be segmented. Therefore as she drives away, the robot may keep the fiducial in view and perform adaptation (as described below) so that anomalies might be observed, and the regions will grow to cover the entirety of the fiducial blocks.

Adaptation helps to cope with dynamic lighting changes that occur after imprinting, such as moving shadows and varying light sources. [3] developed a process for adapting the range of values defining a region in black and white images to provide more accurate region segmentations which can be applied to SCT-based images. The adaptation process uses the current region statistics to predict the parameters for the next segmentation using the formula:

$$range = \bar{x} \pm (n \times SD)$$

\bar{x}, SD are the sample mean and standard deviation, respectively, of SCT angles for pixels segmented for each colored region in a given image frame. Since the noise in the segmented colors does not fit a normal distribution, the standard rubric of using three standard deviations to capture the sample population is not sufficient. Instead, $n = 4$ is used because it provides at least a 93.8% coverage of any distribution, following Chebyshev's Theorem.

To add fault tolerance to the segmentation process, a system to switch between statistical parameter sets was developed. Its operation is summarized in Fig. 5. Assuming the fiducial is found, the statistics are adapted with

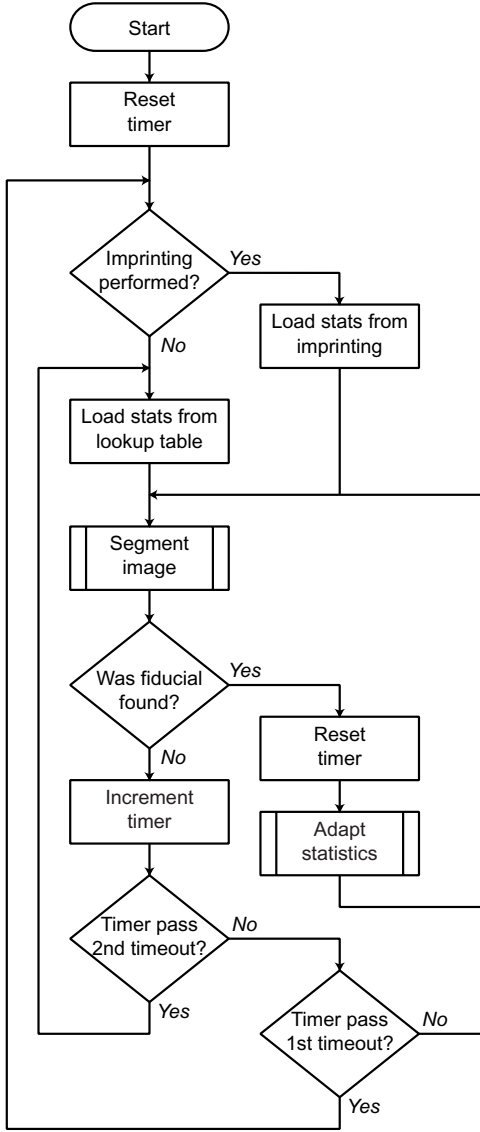


Fig. 5. Parameter selection in the perceptual schema.

each new frame. If the fiducial is not found before the first timeout, it is assumed that adaptation was at fault. Similarly, if the fiducial is not found before the second timeout, it is assumed that imprinting was at fault. In each case, the system reverts to the previous set of statistics. Fig. 7 shows a video frame from the camera, and highlights the pixels that were segmented for each block.

V. IMPLEMENTATION

The close dock behavior was implemented and tested on a marsupial team consisting of Silver Bullet, a modified Power Wheels Jeep, and Bujold, an Inuktun VGTv MicroRover. The pair is shown in Fig. 6. Bujold fits entirely within a compartment, or marsupial pouch, in Silver Bullet. The fiducial is a 18 cm by 11 cm hinged flap covering the entrance to the pouch. The fiducial consisted of two adjacent rectangles, shown in Fig. 7. The rectangles



Fig. 6. The marsupial team, consisting of Silver Bullet, the mother, and Bujold, the daughter.

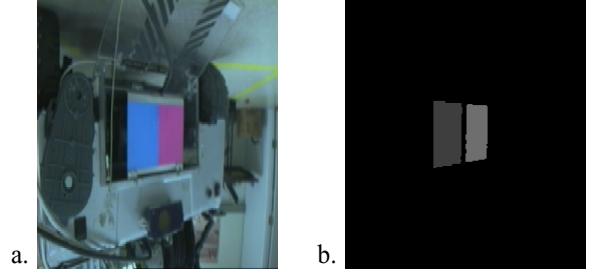


Fig. 7. Fiducial a) as seen, upside down, through the daughter's camera during docking, and b) after segmentation.

were cyan and magenta, opposite colors in SCT space, to simplify vision. Bujold carries no power source or processing capability of her own, but instead uses Silver Bullet's resources via a tether. Although Bujold's processing was done onboard Silver Bullet, the code could equally well be run on the docking agent if this capability existed. The design requires no communication between team members.

One complication of this configuration is that Bujold's tether requires that she back into Silver Bullet, and she must lower herself to fit in the cargo compartment. Within Silver Bullet, the dock size allows for approximately 1 cm of space on each side of Bujold. These tight tolerances are somewhat mitigated, however, by a funneled opening, which can allow for an approach which is up to 15° off axis. In practice, the robot needed to aim for much more precise positioning to compensate for uneven slippage of the tracks on the gate and errors in segmentation. After experimentation, parameters were chosen that would only allow Bujold to dock if she was within about ±2 cm laterally and ±5° off axis.

The lens on Bujold's camera has a full angle field of view of approximately 70°, allowing the entire fiducial to be in view up to the point Bujold encounters Silver Bullet's ramp. These camera parameters also served to limit the docking region to about 2 meters from the fiducial. Onboard Silver Bullet, images were acquired with a Matrox

Meteor framegrabber. Processing was performed on a 400 MHz AMD K6-II. Running the perceptual schema code, Bujold's 256×240 pixel images could be processed at a rate of about 3.25 Hz. The time taken by the SCT takes up more than 80% of each sense-act cycle, at a cost of two floating point divides, two trigonometry operations, and a square root operation per pixel.

The ratio of the left and right pixel counts is sufficient to guide the robot. This ratio, which is calculated so as to be between zero and one, is then mapped into a steering command. Bujold's control is a restricted case of skid steering where she can either turn or drive straight, but not both simultaneously. To accomplish a gradual turn, she alternates between the two. Unfortunately, when the robot is turning, she makes no forward progress. In order to cut down on excessive turning, a dead band was created around straight ahead, and the algorithm purposely understeers. In this portion of the docking process, speed is governed by the summed pixel count of both fiducial blocks.

When the total pixel count exceeds a known threshold, the robot may be either at the dock, or near but off center. At this point, she must make a decision whether to proceed into the mother, or move away to try again. If the ratio of left to right pixel counts is close to one and the fiducial is centered in the image, Bujold will minimize her height and back into the dock. Otherwise, she will move away to center herself.

VI. EXPERIMENTS

In order to test the operation of the docking behavior, two sets of formal experiments were conducted for a total of 254 trials. The first experiment established a baseline of the behavior's motor schema performance under favorable laboratory lighting conditions. The metrics were: *time to dock* and *success rate*. With this experiment, it was found that the vehicle could dock more quickly than and with similar reliability to a human teleoperator. The second experiment tested the behavior's performance in challenging lighting conditions. This experiment was designed to test the benefit of using the combination of adaptation and imprinting over using imprinting alone in real-world lighting scenarios. Again, the metrics were *time to dock* and *success rate*. Results from this experiment showed that adaptive segmentation performs better than static segmentation in outdoor lighting conditions. Additional informal experiments were performed in other lighting conditions. In all cases, the behaviors were autonomous, requiring only a single user command to initiate, while teleoperation averaged 29 commands per meter.

A. General Docking Performance

To evaluate the behavior's basic performance, the daughter's docking time from 16 locations distributed over a field behind the mother was recorded. This field extended to 2 meters, and in 60° either direction off center, as shown in Fig. 8. Although the Approach Zone extends 70° , 60° made the perception more reliable. In all cases, the robot was

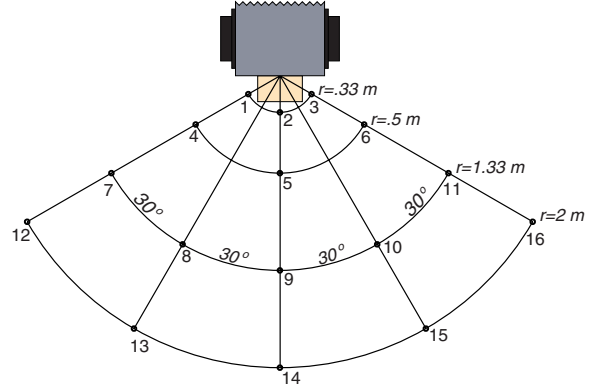


Fig. 8. Autonomous vs. teleoperated docking experiment starting positions.

placed directly facing the fiducial on Silver Bullet. Since the robot rotates until it sees the fiducial, placing it where it did not face the fiducial would simply add time to the beginning of the nominal docking process.

The times and success rate of twenty-two teleoperators attempting manual docking were used as a baseline for the metrics. Sixteen were non-experts, undergraduate volunteers, and six were experts who routinely teleoperated Bujold or another robot at least once a week. Each was given up to fifteen minutes of practice docking the robot while permitted to view the robot as well as the display. The display consisted of a direct video feed from the robot. Since the robot is backing in, the camera images are actually upside-down, as Bujold's camera is tilted 180° . While this may seem unfair, it does result in a system that is self consistent. (By also inverting the control mechanism, driving toward an object while turning left causes the object to move right in the image.) Operators used the same five-function control scheme (forward, backward, right, left, stop) as the system. During the trials, the teleoperator's view of the robot was blocked. Each teleoperator performed three trials, each from one of the sixteen positions, randomly selected by the recording program. Timing was automatic, starting with the presentation of the video signal and ending upon Bujold's contact with pressure plates installed within Silver Bullet's bay.

The mean times for autonomous and teleoperated docking are shown in Table Ia. Note that positions are grouped by symmetry. Table Ib presents these times as a function of angle, and Table Ic presents them as a function of distance. Not surprisingly, docking time increased with both angle and distance. Interestingly, however, teleoperators took longer to dock from 30° than from 60° off-center.

The teleoperators were able to successfully dock in 95% of the 66 trials, with an effective average velocity of 2.0 cm/s. Under autonomous operation, the robot successfully docked in 96% of its 48 trials, with an effective average velocity of 2.4 cm/s. On average, the robot took 17% less time to successfully dock than did a teleoperator. While attempting to dock autonomously, the system missed the dock twice. In such instances, the daughter got stuck on

	Mean Time to Dock (s)	
Position	Autonomous	Teleoperator
1,3	89.2	59.3
2	25.6	21.5
4,6	61.3	70.2
5	39.6	46.5
7,11	64.0	80.7
8,10	59.8	86.7
9	54.3	52.5
12,16	81.6	96.9
13,15	67.5	86.6
14	66.6	52.5

a.

Angle	Mean Time to Dock (s)
0°	46.5
30°	63.6
60°	73.8

b.

Distance (m)	Mean Time to Dock (s)
.33	65.3
.50	54.1
1.33	60.1
2.00	73.0

c.

TABLE I

MEAN TIME TO AUTONOMOUSLY DOCK AS A FUNCTION OF A) STARTING POSITION, B) ANGLE, AND C) DISTANCE

For Locations 1,6,7,10,14	Adaptive / Static	Mean Time to Dock (s)	Success / Failure
Normal Lab Lighting	adaptive	68	.93
	static	not tested	not tested
Emergency Flashers	adaptive	93	.87
	static	84	.93
Outdoors Noon	adaptive	89	.87
	static	106	.53
Outdoors Dusk	adaptive	93	1.00
	static	109	.70

TABLE II

TIME TO DOCK AND SUCCESS RATE AS A FUNCTION OF ADAPTIVE VS. STATIC SEGMENTATION IN VARIOUS LIGHTING CONDITIONS

the edge of the entrance, and stalled. In the interest of robot preservation, such a run was stopped immediately. Three human operators also missed the dock during the dead reckoning phase. When this happened, it necessitated driving forward, changing geometry to bring the mother robot into view, adjusting as necessary, changing the geometry again, and re-attempting the final dead reckoning phase. The run was allowed to continue, but for comparison purposes, these times were not used to compute the mean.

Comparing the data with a paired-sample *t*-test reveals only a 22% chance that human operators can, on average, dock the daughter as quickly as can be done autonomously.

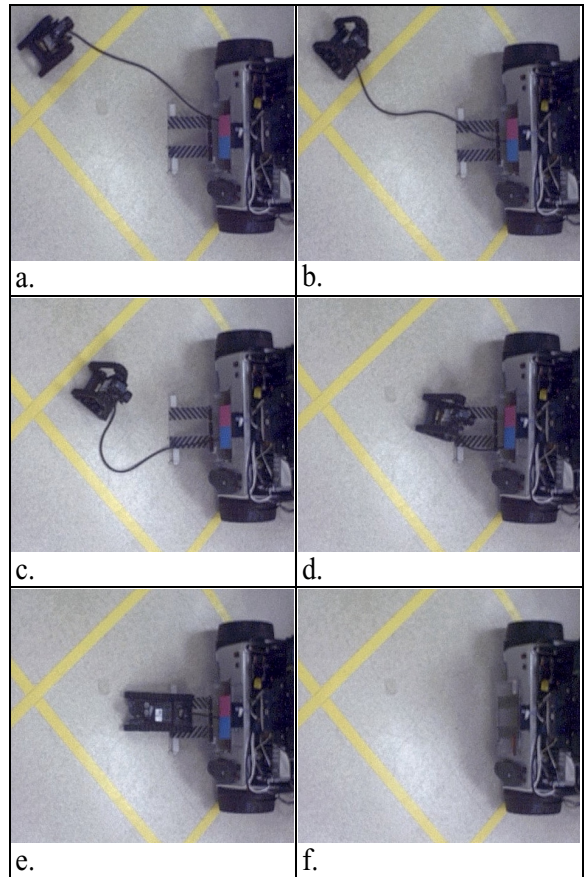


Fig. 9. Bujold docking. She a) begins turned away from the fiducial; b) turns to acquire it; c) approaches; d) stops when at the dock; e) changes geometry and backs in using dead reckoning; and f) triggers Silver Bullet's gate to close.

Furthermore, this may be optimistic given that it was not originally intended for the robot to be able to dock from positions 1 and 3. These positions lie on the border of the Approach Zone, where the robot does not traverse during normal docking maneuvers. They were included because experimentation revealed that the robot would eventually work its way around the corner of the gate by repeatedly moving back and forth. If these positions are dismissed from consideration, the *t*-test result is 0.047, less than a 0.05 significance level.

B. Performance in Challenging Lighting Conditions

The next experiment was intended to measure whether adaptive segmentation performed better than static segmentation under challenging lighting conditions. The metrics used to make this distinction were *time to dock* and *success rate*. Tests were conducted in three lighting conditions: *indoors with emergency flashers*, *outdoors at noon*, and *outdoors at dusk*. In the first, regular lab lighting was left on, but two rotating orange lights designed for emergency vehicles were placed 1.5 m behind and 0.5 m to the left and right of the fiducial. (See Fig.10.) In the following

two, docking *outdoors at noon* began at noon, and continued until the trial set had been exhausted, at 2:00 PM. Docking *outdoors at dusk* began 90 minutes before sunset and proceeded until it was too dark for the system to imprint, 20 runs later.

In each case, test runs were started at five representative locations from the previous experiment (positions 1, 6, 7, 10, and 14 in Fig. 8). Three runs were made from each position, for both adaptive and static segmentation (for a total of 30 data points in a full set for each lighting condition). The procedure was as follows: first, imprinting was performed. Second, a docking position from the list and segmentation method (adaptive or static) are randomly determined. The proctor then places the robot at the starting location, and allows it to dock, the starting time being recorded by the system. A docking attempt was considered a success when the daughter contacted the pressure plates inside the mother, and a failure if she did not do so within 150 seconds. Following this run, another was made from the same position using the remaining segmentation method with the same imprinting statistics. This procedure was repeated for each of the 15 pairs.

The results from the experiment appear in Table II. In indoor lighting, there was no measurable improvement that resulted from using adaptation. It seems that imprinting, which averages the statistics of multiple consecutive frames, provides static segmentation with a surprisingly good measure of (virtual) fiducial color. Additionally, imprinting records the standard deviation of the colors, which was intended to compensate for spatial variations within the patches. However, it also worked in this case to compensate for the rapid periodic temporal variation. Outdoors, adaptive segmentation was found to perform more reliably than static segmentation with a *z*-test result of 0.023 at noon, and 0.030 at dusk.

In addition to success/failure rates, this experiment provided other interesting observations. Data collected outdoors suggested that docking proceeded more quickly when using imprinting, though an insufficient number of runs were executed to achieve a 0.05 significance level while still dismissing the times of unsuccessful runs. Regardless of improvements in time or success rate afforded by using imprinting, it offered significant convenience in being able to go from lab to outdoor lighting conditions (moving the white balance switch on the camera in the process), and yet not having to advise the behavior of any changes.

When static segmentation failed, the common scenario was when the daughter correctly approached to within about 0.5 m, but then lost the fiducial as a result of glare or shadows. Moving clouds caused similar failures to occur over the entire approach zone. Whereas imprinting could average over quickly-varying periodic light modulation as produced by the emergency flashers, it could not cope with the sudden, random changes of significant cloud cover.

C. Additional Experiments

In addition to the experiments comparing time and commands, informal scenarios were carried out to demonstrate

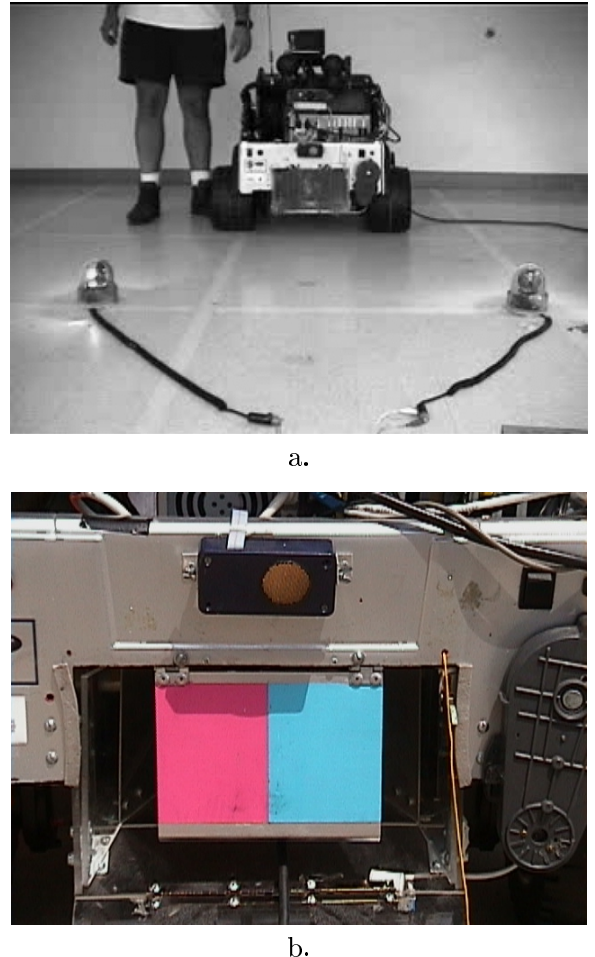


Fig. 10. Examples of challenging lighting conditions used during experiments: a) Flashing emergency lights, b) one of Silver Bullet's sonar unevenly shadows a portion of the fiducial.

the robustness of the system in less reproducible situations. The colors on the fiducial were cyan and magenta. To validate the effect of imprinting, yellow was substituted over either half. Without making any changes to the code, the daughter was able to reliably imprint on the new colors, drive to a random location within the approach zone, and dock as usual. Of course, this relied on the daughter never reverting to table lookup for the color statistics. It does, however, highlight the flexibility of the system.

Adaptation and the ability to fall back through parameter sets to reinitialize appear to be powerful, practical tools. In one instance, the daughter was able to imprint at dawn, go into "sleep" mode, then wake up and dock several hours later, without having imprinted again, but using only adaptation. (See Fig. 11.) Likewise, the daughter was able to dock indoors with moving shadows being cast on the fiducial.

In another experiment, many cyan and magenta objects were placed around the fiducial, so as to add clutter to the image. (See Fig. 12.) One of these objects was an exact copy of the fiducial, but which was placed upside-down. Though the display showed that many of the objects were



a.



b.

Fig. 11. Bujold outdoors: a) imprinting at dawn, and b) using those parameters to successfully dock in the afternoon.

being segmented as the correct colors, the component analysis kept them from being considered part of the fiducial.

VII. CONCLUSION

This article has detailed a vision-based docking behavior that uses direct perception of an unobtrusive artificial landmark which can be visually segmented and analyzed in time that grows linearly with image pixel count. The docking behavior uses a color segmentation algorithm that is lighting insensitive by virtue of the SCT color space, and is made more so by two enhancements, *imprinting* and *adaptation*. The behavior requires no communication between robot team members, making it suitable for tactical situations. In contrast, a teleoperator has to give an average of 29 commands per meter to dock a robot. The behavior is reactive, and based on behavioral schema, assuring compatibility with reactive and hybrid/reactive architectures. Experimentation determined that reactive docking is faster than teleoperated docking, with a statistical confidence greater than 95%. Docking also has a similar success rate to teleoperation (96% vs. 95%). Outdoors at noon and dusk, the failure rate of autonomous docking using adaptation and imprinting is lower than that of docking using



Fig. 12. Bujold docking in an environment cluttered with many objects of the same color as the fiducial.

imprinting alone, also with a statistical confidence greater than 95%. While this article considers the application only to marsupial robots, the technique should be extensible to any team of physically cooperating robots, including reconfigurable robots.

VIII. ACKNOWLEDGMENTS

This work was supported by DARPA award F04701-99-C-0317. The authors would like to thank LTC John Blitch, SAIC, Aaron Gage, and the anonymous reviewers for their feedback and support. In addition, they wish to thank and Mark Powell for his help with the SCT.

REFERENCES

- [1] R. C. Arkin and R. R. Murphy. Autonomous navigation in a manufacturing environment. *IEEE Transactions on Robotics and Automation*, 6(4):445–454, 1990.
- [2] J. Hyams, M. Powell, and R. Murphy. Position estimation and cooperative navigation of micro-rovers using color segmentation. *Autonomous Robots*, 9:7–16, 2000.
- [3] R. R. Murphy. Adaptive tracking for a mobile robot. In *Fifth IEEE International Symposium on Intelligent Control*, pages 1044–1049, Philadelphia, PA, Sept. 1990.
- [4] R. R. Murphy. Marsupial robots for urban search and rescue. *IEEE Intelligent Systems*, 15(2):14–19, 2000.
- [5] P. Questa, E. Grossmann, and G. Sandini. Camera self orientation and docking maneuver using normal flow. In *Proceedings SPIE*, volume 2488, pages 274–283, Orlando, FL, April 17–18 1995.
- [6] H. Roth and K. Schilling. Navigation and docking maneuvers of mobile robots in industrial environments. In *IROS 98*, pages 2458–2462, Aachen Germany, Aug. 31–Sept. 4 1998.
- [7] J. Santos-Victor and G. Sandini. Visual behaviors for docking. *Computer Vision and Image Understanding*, 67(3):223–238, 1997.
- [8] J. Spofford, J. Blitch, W. Klarquist, and R. Murphy. Vision-guided heterogeneous mobile robot docking. In *Proceedings SPIE*, volume 3839, pages 112–121, 1999.
- [9] M.C. Tse and R. Luo. Integrated multi-behavioral mobile robot navigation using decentralized control. In *IROS 98*, pages 564–569, Victoria, BC Canada, Oct. 13–17 1998.
- [10] Scott E. C. Umbaugh. *Computer Vision and Image Processing*. Prentice-Hall, Englewood Cliffs, NJ, 1998.
- [11] J. Vandorpe, H. Xu, and H. Van Brussel. Dynamic docking integrated in a navigation architecture for the intelligent mobile robot Iias. In *IAS 95*, pages 143–149, Karlsruhe Germany, March 27–30 1995.